J. Iron Steel Res. Int.
https://doi.org/10.1007/s42243-024-01294-3

ORIGINAL PAPER

Isothermal reduction kinetics and reduction prediction for iron ore pellets

Fei Meng[1] · Hao Liu[1,2,3] · Yue-lin Qin[1] · Huang-jie Hua[1] · Yin Deng[1] · Ze-zheng Sun[1] · Long-hai Liu[4]

Received: 21 December 2023 / Revised: 4 February 2024 / Accepted: 6 March 2024

Abstract
Iron ore pellets, as one of the main charges of blast furnaces, have a greater impact on the CO_2 emission reduction and stable operation of blast furnaces. The isothermal reduction behavior of the pellets obtained from a Chinese steel plant was studied in the gas mixtures of CO and N_2. The results showed the reduction process is divided into two stages. The reduction in the initial stage (time $t \leq 40$ min) is cooperatively controlled by internal diffusion and interface chemical reactions with the activation energy of 30.19 and 16.67 kJ/mol, respectively. The controlling step of the reduction in the final stage ($t > 40$ min) is internal diffusion with the activation energy of 34.60 kJ/mol. The reduction process can be described by two equations obtained from kinetic calculations. The reduction degree can be predicted under different temperatures and time, and the predicted results showed an excellent correlation with the experimental results. The reduction mechanisms were confirmed by the analysis of the scanning electron microscope equipped with an energy dispersive spectrometer and optical microscope.

Keywords Pellet · Reduction behavior · Kinetics · Mechanism · Reduction prediction

1 Introduction

As a basic material, steel is widely used in various industries in today's society. In China, the steel industry process is dominated by the carbon-intensive blast furnace–basic oxygen furnace (BF–BOF) process, which accounts for about 15% of Chinese total CO_2 emissions [1–3]. The pig iron production from the blast furnace accounts for 90% of the total pig iron production in China, and the CO_2 emission from the blast furnace ironmaking process accounts for 62% of the total iron production process [4, 5]. Under the current global CO_2 emission reduction policy requirements, CO_2 emission reduction in the ironmaking process has become a focus of attention. Due to the good mechanical and metallurgical properties of pellets, such as uniform particle size, high cold strength, high iron grade, low energy consumption, and low pollutant emission, pellets are considered one of the best charges for blast furnaces [6]. Furthermore, with the gradual depletion of high-grade raw materials, the steel industry is forced to use low-grade ores with high levels of harmful elements [7, 8]. Low-grade iron ore requires a beneficiation process to increase the iron grade and remove harmful impurity elements. Pelletizing is considered as one of the suitable processes to use iron ore fines after beneficiation. Therefore, the development of a blast furnace charge structure based on pellets and the study of pellets reduction characteristics in the blast furnace are of great significance for reducing CO_2 emissions in the ironmaking process and ensuring stable production in the blast furnace.

Currently, a lot of researchers have studied the reduction behavior and mechanism of pellets by CO [9, 10], pure H_2 [11–13], H_2 and CO/N_2 mixtures [14–16], coal [17–19],

✉ Hao Liu
liuhao@cqust.edu.cn

✉ Yue-lin Qin
qinyuelin710@163.com

1 School of Metallurgy and Materials Engineering, Chongqing University of Science and Technology, Chongqing 401331, China

2 CISDI Group Co., Ltd., Chongqing 401122, China

3 College of Materials Science and Engineering, Chongqing University, Chongqing 400044, China

4 Sichuan Desheng Group Vanadium & Titanium Co., Ltd., Leshan 614000, Sichuan, China

Published online: 13 August 2024

and biochar [20–22]. Although various mechanistic models have been used to explain the reduction behavior well, most of the studies have focused on the reduction behavior of laboratory-made pellets, briquettes, or iron ore powders, but fewer studies have been conducted to investigate the reduction behavior of pellets produced on-site at steel companies. Nevertheless, most of these studies are performed with pure reducing gas or solid reducing agent, which is not representative of the actual reduction atmosphere in the lumpy zone of BF, where descending ores react with the counter reducing gas flow.

In this study, the reduction behavior of the pellets produced on-site at a Chinese steel company was investigated under different temperatures and time with the gas mixtures of CO and N_2. The kinetics of the reduction process were also evaluated with the shrinking unreacted core model, and the reduction degree of pellets was also predicted based on the reaction equation obtained from kinetic calculations. At last, the analysis of the X-ray diffraction (XRD), scanning electron microscopy with energy dispersive spectrometry (SEM–EDS), and optical microscopy was adopted to verify the reduction mechanisms of pellets.

2 Experimental

2.1 Materials

The iron ore pellets used in this study were supplied by Shougang Qianan Steel Company (China). The major chemical composition of the pellets is shown in Table 1. To reveal the transformation of the physical phase of the pellets, a SmartLab-9 X-ray diffractometer with Cu Kα radiation (wavelength $\lambda = 0.179$ nm), acceleration voltage of 45 kV, and current of 30 mA was used to determine the phases present in the original and reduced pellets. The XRD results indicate that the original pellets are mainly composed of hematite (Fe_2O_3), with minor amounts of silicate (Fig. 1).

2.2 Experiments

The whole reduction experiment was carried out in a variable atmosphere-programmed heating reduction apparatus, which consists of a heating furnace, reduction tube,

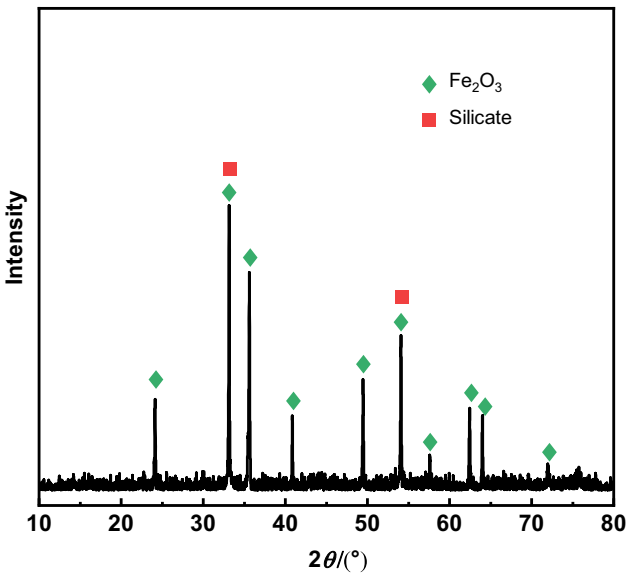

Fig. 1 XRD patterns of original pellets. 2θ—Diffraction angle

control system, and weighing system with an accuracy of 0.1 g (Fig. 2). 500 g pellets were placed in the reduction tube (ϕ75 mm × 80 mm, made of heat-resistant steel) and heated from ambient temperature to a target temperature at a heating rate of 20 °C/min under 5 L/min N_2 stream. Upon reaching the desired reaction temperature, the N_2 flow rate was increased to 15 L/min and this temperature was maintained for around 30 min. Then, the reducing gas mixture (30% CO–70% N_2) was introduced at a total flow rate of 15 L/min for 180 min. Before moving out from the furnace and transferring to sealed capsules for additional analysis, the reduced pellets were cooled to room temperature under an N_2 atmosphere at the flow rate of 5 L/min. The mass loss of the pellets during the experiment was recorded continuously by connecting an automatic high-precision balance to a computer. To eliminate errors, each experiment was repeated three times with an error of less than 5%, and the average data of the three groups was selected. The optical microscope (DM1750M, Leica Microsystems, Wetzlar, Germany) was employed to characterize the microstructure of the original and reduced pellets. The phases and microstructure of the reduced pellets were examined using an SEM (JSM-7800F, JOEL, Japan) with an EDS and an XRD (SmartLab-9, Rigaku, Japan), respectively.

Table 1 Major chemical composition of iron ore pellets

R_2	TFe/wt.%	SiO_2/wt.%	CaO/wt.%	FeO/wt.%	Al_2O_3/wt.%	MgO/wt.%	S/wt.%	P/wt.%
0.32	61.21	5.18	1.65	2.56	1.44	1.06	0.01	0.05

$R_2 = w(CaO)/w(SiO_2)$; TFe—total iron

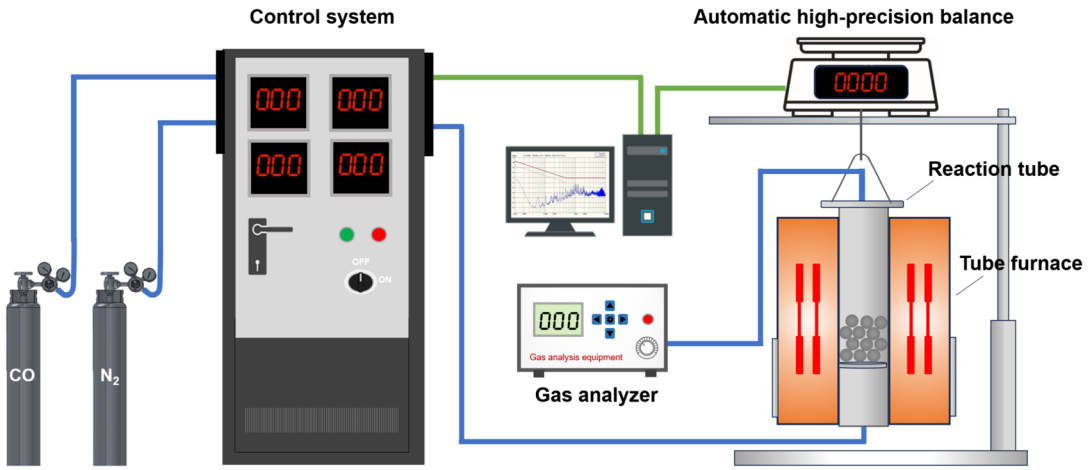

Fig. 2 Schematic diagram of reduction simulator

Isothermal reaction kinetics were investigated by varying the reaction temperature (800–1000 °C) and the reduction time (0–180 min). The degree of reaction is calculated by Eq. (1) from the Chinese national standard GB/T 13241–2017:

$$R = \left(\frac{0.111w_{\mathrm{FeO}}}{0.430w_{\mathrm{TFe}}} + \frac{m_1 - m_t}{m_0 \times 0.430w_{\mathrm{TFe}}}\right) \times 100\% \quad (1)$$

where R is the reduction degree, %; m_0 is the mass of the original pellets, g; m_1 is the mass of the pellets at the beginning of reduction, g; m_t is the mass of pellets after reaction for time t, g; w_{FeO} is the FeO content in the pellets, %; and w_{TFe} is the total iron content in the pellets, %.

3 Results and discussion

3.1 Reduction behavior

The effects of reduction temperature and time on the reduction behavior of pellets were investigated at 800–1000 °C for 180 min under the reducing gas mixtures of 30% CO–70% N_2, and the results are illustrated in Fig. 3. As shown in Fig. 3, the reduction of pellets is obviously affected by temperature. An increase in the reduction temperature greatly improves the reduction of pellets. As the temperature increased from 800 to 1000 °C, the reduction of pellets improved rapidly from about 53% to 69%. The improvement of the reduction degree with temperature could be attributed to the fact that increasing temperature can lead to an increase in the diffusion rate of reducing gases and the rate of chemical reaction [18].

As can be seen in Fig. 3, the reduction rates of pellets are faster in the early stage, and then, the reduction rate gradually decreases. To understand the specific variation of the reduction rate, the data in Fig. 3 are derived to obtain

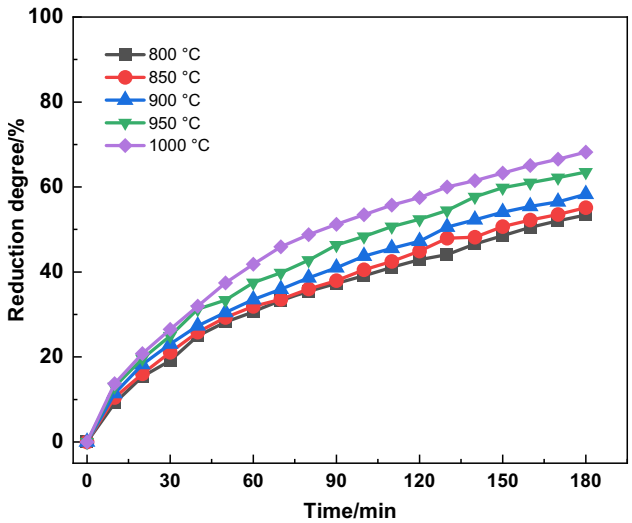

Fig. 3 Effect of temperature and time on reduction of pellets

the curve of the reduction rate. The results are shown in Fig. 4. As shown in Fig. 4, in the whole reduction process, the reduction rate of pellets at high temperatures is higher than that at lower temperatures.

In addition, a significant decrease in the reduction rate was observed with the increase in reduction time. The reduction rate in the initial stage is notably higher than that in the final stage. This indicates that the reduction rate is obviously divided into two stages with the increase in reaction time. When the reduction time is less than 40 min, the reduction of pellets is fast. As the reduction time is higher than 40 min, the reduction process is relatively slow. As mentioned above, the pellets are mainly composed of Fe_2O_3, and its reduction sequence is $Fe_2O_3 \rightarrow Fe_3O_4 \rightarrow FeO \rightarrow Fe$. The reduction of Fe_2O_3 to FeO is remarkably easier than that of FeO to Fe; thus, the reduction rate in the initial stage is very high [23]. Furthermore, in the initial stage, the outer product layer of the pellet is

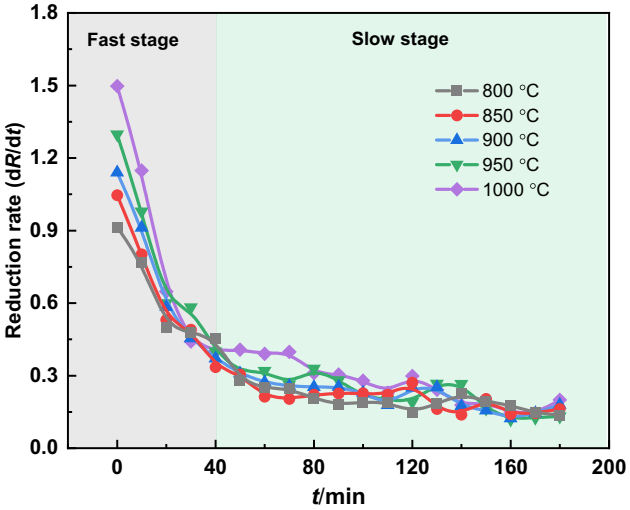

Fig. 4 Effect of reduction temperature on reduction rate

thin, and as the reduction time increases, the product layer gradually becomes thicker, which may cause resistance to the diffusion of the reducing gases and lead to a lower reduction rate [13].

3.2 Kinetics and mechanism of reduction

To determine the mechanism of pellet reduction, kinetic analyses were carried out during the reduction process. The reduction of pellets is a solid–gas two-phase process system, and the reaction is considered to occur on the surface of the unreacted pellets. The shrinking unreacted core model is widely applied to describe the kinetics and mechanism of iron oxide pellet reduction by gas mixtures. According to the shrinking unreacted core model, the chemical reaction starts from the surface of the solid phase and gradually advances to the center, a layer of solid-phase products will be formed, and there is an obvious interface between the unreacted part and the product layer, while the inner core of the solid phase is the unreacted part. The reduction of the solid–gas two-phase process has three parts: (1) the gas diffused to reach/leave the surface of pellets through the gas phase boundary layer (external diffusion), (2) the gas diffusion to reach/leave the surface of the unreacted core through the reduction product layer (internal diffusion), and (3) the interface reduction reaction of iron oxide (interface chemical reaction). The step with larger resistance is considered as the controlling step of the reduction process. As the gas velocity adopted in this experiment is relatively high, the external diffusion is not considered as a controlling step. Thus, the reduction process of pellets may be controlled by: (1) internal diffusion, (2) interface chemical reaction, and (3) cooperative control of internal diffusion and interface chemical reaction.

The solid–gas reaction is commonly described as [24]:

$$\frac{(c_0 - c_e)}{r_0^2 \rho} t = \frac{1}{6D_e}[3 - 2R - 3(1-R)^{2/3}] + \frac{1}{kr_0}[1 - (1-R)^{1/3}] \quad (2)$$

where r_0 is the radius of the pellet, m; ρ is the molar density of the pellet, mol/m^3; c_0 is the original concentration of the reducing gas, mol/L; c_e is the concentration of the reducing gas at reaction equilibrium, mol/L; D_e is the gas internal diffusion coefficient; and k is the chemical reaction equilibrium constant.

(1) When the interface chemical reaction acts as a controlling step, i.e., k is much smaller than D_e ($k << D_e$), which means that $1/D_e$ is negligible, Eq. (2) can be simplified to Eq. (3).

$$k_r t = 1 - (1-R)^{1/3} \quad (3)$$

where k_r is the interfacial chemical reaction rate constant, $k_r = \frac{k(c_0 - c_e)}{r_0 \rho}$. If the plot of $1 - (1-R)^{1/3}$ versus t is linear, the reduction process is controlled by interfacial chemical reaction, and the slope of the linear plot is k_r.

(2) When the internal diffusion acts as a controlling step, i.e., D_e is much smaller than k ($D_e << k$), which indicates that $1/k$ is negligible, Eq. (2) can be simplified to Eq. (4).

$$k_d t = 1 - 3(1-R)^{2/3} + 2(1-R) \quad (4)$$

where k_d is the internal diffusion rate constant, and $k_d = \frac{2D_e(c_0 - c_e)}{r_0^2 \rho}$. If the plot of $1 - 3(1-R)^{2/3} + 2(1-R)$ versus t is linear, the reduction process is controlled by internal diffusion, and the slope of the linear plot is k_d.

(3) When the resistance of internal diffusion and interfacial reactions are comparable, it implies that both k and D_e need to be considered in the reduction, and the reduction process is cooperatively controlled by internal diffusion and interface chemical reactions. Both sides of Eq. (2) are divided by $1 - (1-R)^{1/3}$ to obtain Eq. (5).

$$\frac{t}{1 - (1-R)^{1/3}} = \frac{1}{k'_d}[1 + (1-R)^{1/3} - 2(1-R)^{2/3}] + \frac{1}{k_r} \quad (5)$$

where $k'_d = \frac{6D_e(c_0 - c_e)}{r_0^2 \rho}$. k_d and k_r can be obtained by plotting $\frac{t}{1-(1-R)^{1/3}}$ versus $1 + (1-R)^{1/3} - 2(1-R)^{2/3}$, and the slope and intercept are $1/k_d$ and $1/k_r$, respectively.

Based on the data in Fig. 2, the plots of $1 - (1-R)^{1/3}$ versus t, $1 - 3(1-R)^{1/3} + 2(1-R)$ versus t, and $\frac{t}{1-(1-R)^{1/3}}$ versus $1 + (1-R)^{1/3} - 2(1-R)^{2/3}$ are shown in Fig. 5. As shown in Fig. 5, all models failed to fit the overall kinetic data, which indicates that the reaction mechanism changes throughout the reaction process. As

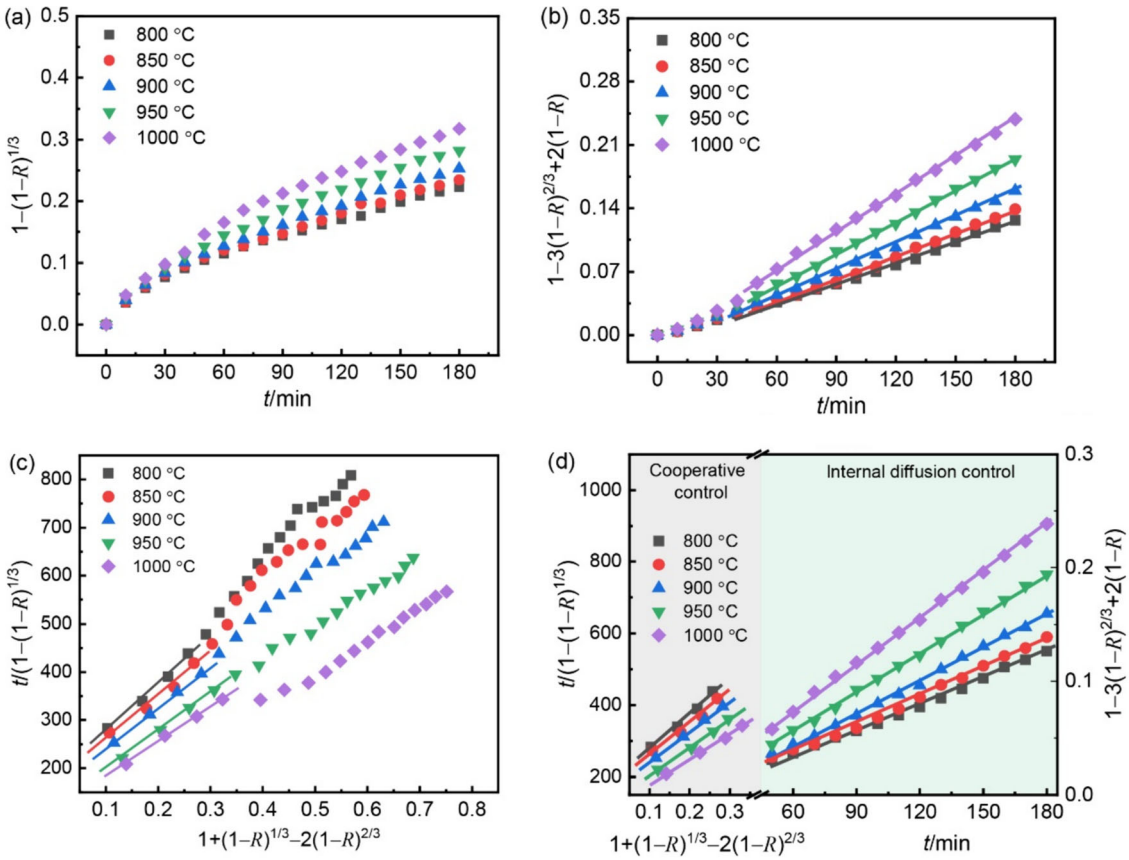

Fig. 5 Model fitting curve for reduction of pellets under different temperatures. **a** Interface chemical reaction; **b** internal diffusion; **c** cooperative control; **d** whole control step

mentioned above, the reaction process is divided into two stages: the fast stage ($t \leq 40$ min) and the slow stage ($t > 40$ min). Therefore, the two stages of the reduction were modeled separately, and the results are shown in Fig. 5d. As shown in Fig. 5d, when the reaction time is less than 40 min, the cooperative control model shows the best linear relationship among the three models with correlation coefficients $R^2 > 0.981$ (Table 2). As the reaction time is higher than 40 min, the internal diffusion model is remarkably suitable to describe the reaction process with $R^2 > 0.995$. Hence, in the initial 40 min, pellets reduction is controlled by a cooperative control of the interfacial chemical reaction and the internal diffusion, and beyond 40 min, the controlling step is the internal diffusion.

All kinetic parameters of internal diffusion rate constant and cooperative control rate constant are calculated and listed in Table 2. All rate constants improve gradually with the increase in reduction temperature, which indicates that the increase in reduction temperature can increase the diffusion rate of reducing gases and the rate of chemical reaction and improve the reduction degree of pellets. In addition, the value of the internal diffusion rate

Table 2 Kinetic parameters for reaction of pellets under different temperatures

Temperature/°C	Cooperative control			Internal diffusion control	
	k'_d/min^{-1}	k_r/min^{-1}	R^2	k_d/min^{-1}	R^2
800	1.00×10^{-3}	5.73×10^{-3}	0.996	0.75×10^{-3}	0.996
850	1.14×10^{-3}	5.72×10^{-3}	0.981	0.83×10^{-3}	0.995
900	1.16×10^{-3}	6.52×10^{-3}	0.995	0.96×10^{-3}	0.996
950	1.24×10^{-3}	8.74×10^{-3}	0.997	1.17×10^{-3}	0.997
1000	1.38×10^{-3}	9.07×10^{-3}	0.998	1.36×10^{-3}	0.998

($k'_d = 1.0 \times 10^{-3} - 1.38 \times 10^{-3}$) in the initial stage is higher than that of the final stage ($k_d = 0.75 \times 10^{-3} - 1.36 \times 10^{-3}$). This implies that the resistance of reducing gas diffusion in the final stage is larger, resulting in a lower reduction rate. This agrees with the experimental results presented in Figs. 3 and 4.

The relationship between the reaction rate constant and temperature can be expressed by the Arrhenius equation below.

$$k = Ae^{-\frac{E_a}{R_0 T}} \tag{6}$$

where A is the frequency factor; E_a is the apparent activation energy, J/mol; R_0 is the universal gas constant, 8.314 J/(mol K); and T is the absolute temperature, K. The activation energies of the reduction reactions can be described by the linear form of the Arrhenius equation, as follows:

$$\ln k = \ln A - \frac{E_a}{R_0 T} \tag{7}$$

Based on the data in Table 2, plots of ln$k$ versus $1/T$ are shown in Fig. 6, and E_a and A values for each stage were determined by the plot. As can be seen from Fig. 6, in the initial stage, the activation energy for the interfacial chemical reaction and the internal diffusion is 30.19 and 16.67 kJ/mol, respectively. The activation energy for the internal diffusion in the final stage is 34.60 kJ/mol. The relatively high value of the activation energy for the internal diffusion in the final stage further confirmed that the resistance of reducing gas diffusion in the final stage is larger, and the reduction process is controlled by internal diffusion.

k_r and k_d of each stage can be obtained by substituting the values of E_a and A into Eq. (6). Substituting k_r and k'_d into Eq. (5), the reaction equation of reduction process in the initial stage ($t \leq 40$ min) takes the form given in Eq. (8).

$$\frac{t}{1-(1-R)^{1/3}} = 152.78e^{\frac{2005}{T}}[1+(1-R)^{1/3} - 2(1-R)^{2/3}] + 6.39e^{\frac{3632}{T}} \tag{8}$$

After replacing k_d in Eq. (4) with the Arrhenius equation, the reaction equation of the reduction process in the final stage ($t > 40$ min) can be described by Eq. (9).

$$0.035e^{-\frac{4162}{T}}t = 1 - 3(1-R)^{1/3} + 2(1-R) \tag{9}$$

In this study, the reduction of pellets under each temperature can be described by combining Eqs. (8) and (9). Thus, the predicted reduction degree under different temperatures and time can be calculated by Eqs. (8) and (9). The results are shown in Fig. 7. As can be seen from Fig. 7, the calculated results are close to the experimental data.

3.3 Characterization

Optical microstructures of original pellets and reduced pellets at 900 °C for 180 min are shown in Fig. 8. Figure 8a indicates that the original pellet is tightly structured with some small pores and mainly consists of Fe_2O_3 and a small amount of silicate. Lots of metallic Fe particles are observed in the edge of reduced pellets and are distributed in the wustite (FeO) matrix (Fig. 8b). The pores in the edge of reduced pellets are larger than those of the original pellets, and the metallic Fe particles appear near the pores. This indicates that the reducing gas is easily diffused through the outer shell of pellets, and iron nucleates and grows on the surface of the wustite particles, leading to the development of the iron–wustite intergrowth layer with a denser structure. The resistance of reducing gas diffusion

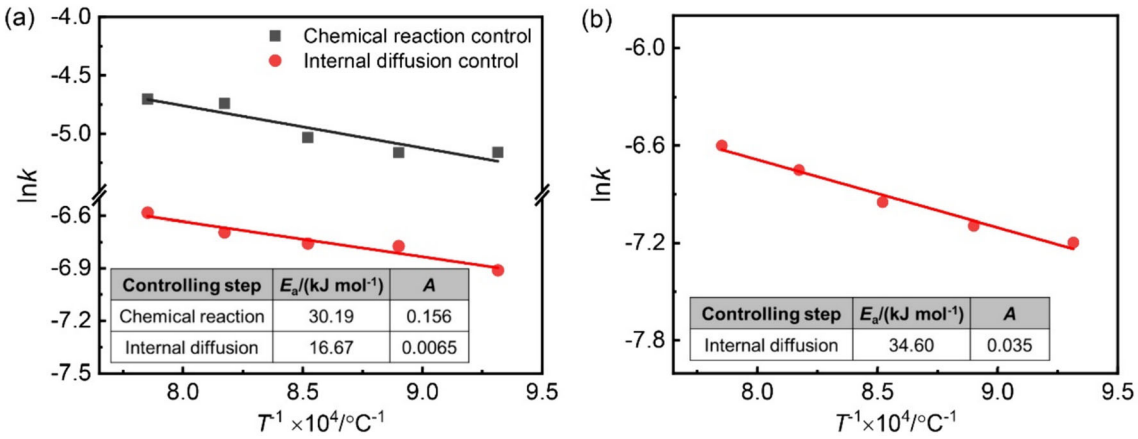

Fig. 6 Arrhenius plots and activation energy for two-stage reduction of pellets. **a** Cooperative control; **b** internal diffusion

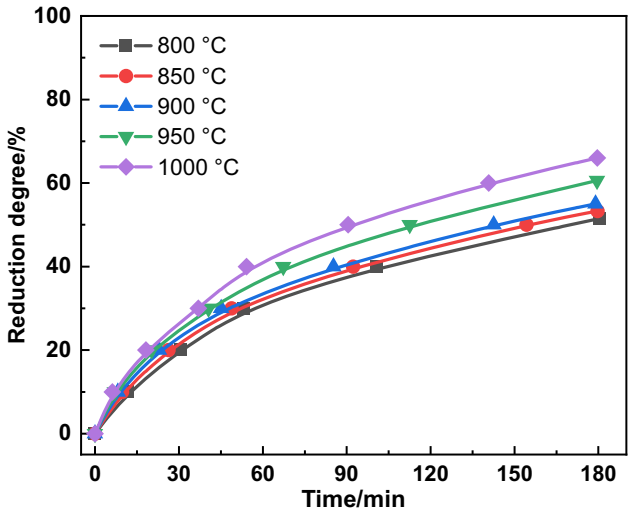

Fig. 7 Calculated reduction degree under different temperatures and time

increases near the iron–wustite intergrowth layer and the reduction of FeO to Fe is significantly difficult. This implies that the reduction process in the initial stage is cooperatively controlled by internal diffusion and interface chemical reactions. As shown in Fig. 8c, d, the amount and size of metallic Fe particles decrease gradually from the inner to the core of reduced pellets, and the metallic Fe particles almost disappear in the core. In addition, fewer pores in the inner and core of reduced pellets are observed, and all of them are in the form of micropores. This indicates that the gas diffusion through the inner layer is the main controlling step and verifies that the reduction process in the final stage is controlled by internal diffusion.

The XRD patterns of the original pellets and the reduced pellets at different temperatures for 180 min are shown in Fig. 9. From the phase identification, it is clearly shown that the original pellets mainly consist of Fe_2O_3 and silicate (Fe_2SiO_4), and the reduced pellets are composed of metallic Fe, FeO, and silicate (Ca_2SiO_4). As the reduction temperature improves, the diffraction intensities of the Fe peak gradually increase, while those of the FeO peak gradually decrease, indicating that increasing the temperature favors the reduction of FeO. Si in the original pellets is mainly in the form of Fe_2SiO_4, while Si in the reduced pellets is mainly in the form of Fe_2SiO_4. When the temperature exceeds 800 °C, Fe_2SiO_4 disappears completely.

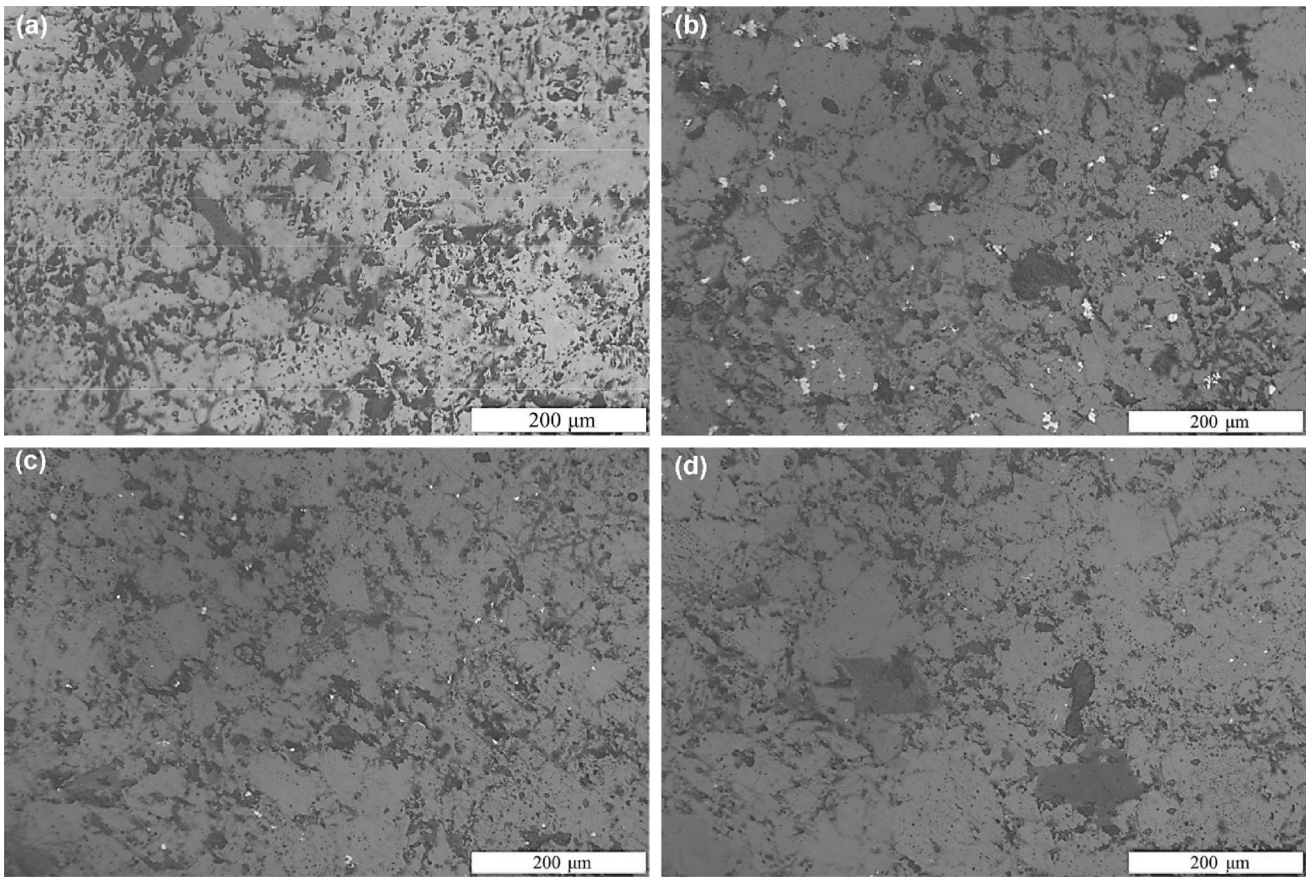

Fig. 8 Photomicrographs of original pellet (**a**), and edge (**b**), inner (**c**), and core (**d**) of reduced pellets at 900 °C for 180 min. Bright white—Fe; ash gray—Fe_2O_3; gray—FeO; dark gray—silicate; black—pore

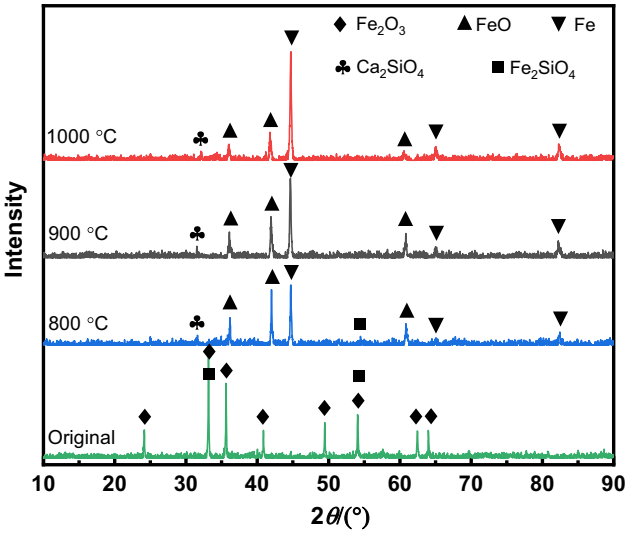

Fig. 9 XRD patterns of original pellets and pellets after reduction for 180 min

This may be due to the gradual reduction of Fe_2SiO_4 at high temperatures, and SiO_2 combines with CaO to form silicates.

Figure 10 shows the SEM–EDS analysis of the reduced pellets under different temperatures (800, 900, and 1000 °C) for 180 min. Based on the percentage of each element and the SEM maps, it is confirmed that the reduced pellets under different temperatures are mainly composed of FeO and a small amount of silicate. Furthermore, the proportion of iron rises significantly with the increase in reduction temperature, which is consistent with the experimental results.

4 Conclusions

1. Temperature plays an important role in the reduction process of pellets which is divided into two stages. The reduction rate in the initial stage ($t \leq 40$ min) is much higher than that of the final stage ($t > 40$ min).
2. The reduction process of pellets in the initial stage is cooperatively controlled by internal diffusion and interface chemical reactions with the activation energies of 30.19 and 16.67 kJ/mol, respectively. The controlling step of the reduction process in the final stage is internal diffusion with an activation energy of 34.60 kJ/mol.
3. The reduction of pellets under different temperatures can be described by combining two equations as follows: Initial stage: $\frac{t}{1-(1-R)^{1/3}}=152.78e^{\frac{2005}{T}}[1+(1-R)^{1/3}-2(1-R)^{2/3}]+6.39e^{\frac{3632}{T}}$. Final stage: $0.035e^{-\frac{4162}{T}}t=1-3(1-R)^{1/3}+2(1-R)$. The predicted results calculated from these two equations show an excellent correlation with the experimental results.
4. The reduction mechanisms of pellets are confirmed by the analysis of the XRD, SEM–EDS, and optical microscopy. The resistance of gas internal diffusion and chemical reaction in the initial stage is both

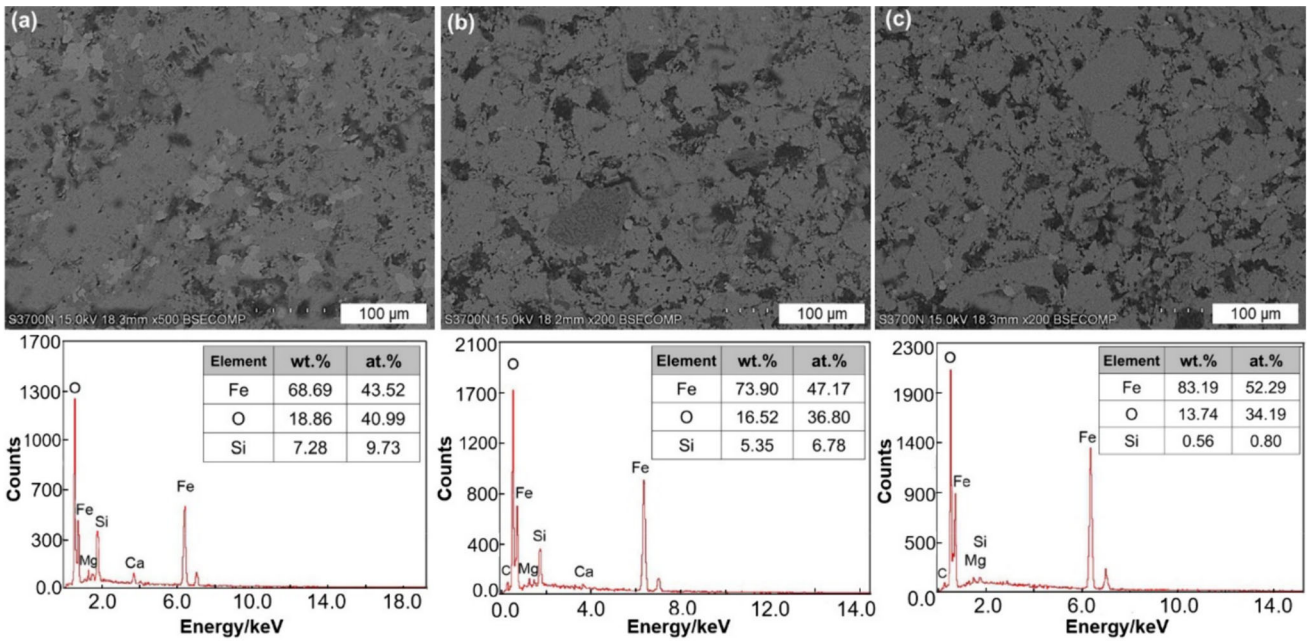

Fig. 10 SEM–EDS analysis of pellets after reduction for 180 min. **a** 800 °C; **b** 900 °C; **c** 1000 °C

relatively high. In the final stage, the resistance of gas internal diffusion dominates the reduction.

Acknowledgements The authors would like to extend their thanks to the financial support from the National Natural Science Foundation of China (No. 52174300), Natural Science Foundation of Chongqing, China (Nos. cstc2020jcyj-msxmX0583 and cstc2021jcyj-msxmX1004), Chongqing Talent Plan Project (No. cstc2021ycjh-bgzxm0211), and Chongqing Doctoral "Through Train" Project (No. sl202100000343). The valuable suggestions from reviewers are also gratefully acknowledged.

Declarations

Conflict of interest The authors declare that they no conflict of interest.

References

[1] S. Zhang, B. Yi, F. Guo, P. Zhu, J. Clean. Prod. 340 (2022) 130813.
[2] W. Sun, Q. Wang, Z. Zheng, J. Cai, Energy Convers. Manag. 213 (2020) 112828.
[3] Z. Wen, Y. Wang, H. Li, Y. Tao, D. De Clercq, J. Environ. Manage. 246 (2019) 717–729.
[4] Z.Y. Wang, D. Han, Z.G. Liu, M.S. Chu, Y.J. Zhang, L.F. Zhang, J.W. Bao, M.Y. Wang, J. Iron Steel Res. Int. 30 (2023) 2163–2172.
[5] Y. Wang, H. Zuo, J. Zhao, Ironmak. Steelmak. 47 (2020) 640–649.
[6] J. Lei, X. Gao, J.S. An, G.D. Bao, Y.Q. Kong, H.M. Long, J. Iron Steel Res. Int. 30 (2023) 2143–2152.
[7] J.A. Halt, M.C. Nitz, S.K. Kawatra, M. Dubé, Miner. Process. Extr. Metall. Rev. 36 (2015) 258–266.
[8] M. Iljana, A. Kemppainen, T. Paananen, O. Mattila, E. Pisilä, M. Kondrakov, T. Fabritius, Int. J. Miner. Process. 141 (2015) 34–43.
[9] N. Dilmaç, Fuel 296 (2021) 120707.
[10] M.I. Nasr, A.A. Omar, M.M. Hessien, A.A. Ei-Geassy, ISIJ Int. 36 (1996) 164–171.
[11] D. Guo, M. Hu, C. Pu, B. Xiao, Z. Hu, S. Liu, X. Wang, X. Zhu, Int. J. Hydrog. Energy 40 (2015) 4733–4740.
[12] A. Bhaskar, M. Assadi, H. Nikpey Somehsaraei, Energies 13 (2020) 758.
[13] A. Hammam, Y. Li, H. Nie, L. Zan, W. Ding, Y. Ge, M. Li, M. Omran, Y. Yu, Min. Metall. Explor. 38 (2021) 81–93.
[14] H.B. Zuo, C. Wang, J.J. Dong, K.X. Jiao, R.S. Xu, Int. J. Miner. Metall. Mater. 22 (2015) 688–696.
[15] M. Bai, H. Long, L. Li, D. Liu, S.B. Ren, C.F. Zhao, J. Cheng, Int. J. Hydrog. Energy 43 (2018) 15586–15592.
[16] W. Li, G.Q. Fu, M.S. Chu, M.Y. Zhu, J. Iron Steel Res. Int. 24 (2017) 34–42.
[17] R.K. Dishwar, O.P. Sinha, Fuel 296 (2021) 120640.
[18] Y. Man, J.X. Feng, F.J. Li, Q. Ge, Y.M. Chen, J.Z. Zhou, Powder Technol. 256 (2014) 361–366.
[19] Y. Shi, Z. Guo, D. Zhu, J. Pan, S. Lu, J. Alloy. Compd. 953 (2023) 170126.
[20] A.T. Ubando, W.H. Chen, H.C. Ong, Energy 180 (2019) 968–977.
[21] Q. Hu, D. Yao, Y. Xie, Y. Zhu, H. Yang, Y. Chen, H. Chen, Energy Convers. Manag. 158 (2018) 1–8.
[22] D. Guo, L. Zhu, S. Guo, B. Cui, S. Luo, M. Laghari, Z. Chen, C. Ma, Y. Zhou, J. Chen, B. Xiao, M. Hu, S. Luo, Fuel Process. Technol. 148 (2016) 276–281.
[23] R.J. Fruehan, Metall. Trans. B 8 (1977) 279–286.
[24] J. Szekely, J.W. Evans, H.Y. Sohn, Gas–solid reactions, Academic Press, New York, USA, 1976.